ACS APPLIED MATERIALS & INTERFACES

Research Article

www.acsami.org

Glucose-Promoted Zn-Based Metal–Organic Framework/Graphene Oxide Composites for Hydrogen Sulfide Removal

Zheng-Hong Huang,*[,†] Guoqiang Liu,[†,§] and Feiyu Kang*[,†,‡]

[†]Laboratory of Advanced Materials, Department of Materials Science and Engineering, Tsinghua University, Beijing 100084, People's Republic of China

[‡]Institute of Advanced Materials Research, Graduate School at Shenzhen, Tsinghua University, Shenzhen 518055, People's Republic of China

Supporting Information

ABSTRACT: Zinc-based metal–organic frameworks/graphene oxide (MOF-5/GO) composites were synthesized via the solvothermal method. The materials were characterized by scanning electron microscopy (SEM), nitrogen adsorption, X-ray diffraction (XRD), Fourier transform infrared (FTIR) spectroscopy, and X-ray photoelectron spectroscopy (XPS), and their performances for hydrogen sulfide (H_2S) removal were evaluated by dynamic testing at room temperature. The composites exhibit microporous structure with a small amount of mesopores, and the structure is highly dependent on the amount of GO loaded. The surface area and pore volume first increase and then decrease with increasing GO, reaching the maximum value when the GO ratio is 5.25%. The composites exhibit high adsorption capacities for H_2S, with the maximum uptakes reaching up to 130.1 mg/g. Although the loading of GO makes a contribution to the enhancement of dispersive force in the porous structure, it leads to the crystal distortion of MOF-5. The introduction of glucose can restrain this distortion to maintain the structure stability. A good match between GO and glucose have a well synergy effect to develop the porous structure, resulting in the highest H_2S adsorption capacity.

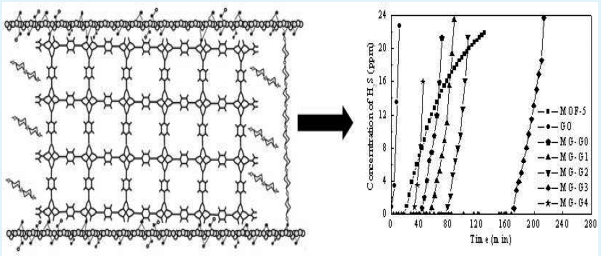

KEYWORDS: *metal–organic frameworks, graphene oxide, glucose, composites, desulfurization, hydrogen sulfide*

1. INTRODUCTION

Hydrogen sulfide (H_2S) is one of the most harmful components arising from many industrial activities such as biogas,[1] petroleum refining,[2] coal gasification,[3] food processing and livestock farming,[4] natural gas processing,[5] geothermal wells,[6] and municipal sewage treatment facilities.[7] The emissions of H_2S have been associated with the formation of acid rain and many other undesirable environmental and health hazards. At levels up to 30–40 ppmv, H_2S can cause acute poisoning, instantaneous loss of consciousness, and rapid apnea, while even death may result from acute exposure to H_2S at levels of 100–200 ppmv.[8] Therefore, controlling their emissions has become increasingly urgent and important for global atmospheric chemistry and quality of life.[9]

Many researchers have been performing experiments and simulations to develop effective technologies for reducing H_2S emissions, and using solid adsorbent is a promising approach for the removal of H_2S. To evaluate the practicality of a solid adsorbent, the following characteristics must be considered: porosity, structural stability, reversible uptake and release, and capability for surface modification for creating molecule-specific adsorption sites.[10] As far as we know, some disadvantages such as low adsorption capacity, flammability, and other problems associated with regeneration for most common porous materials are encountered in practical applications.[11] Therefore, much attention has been paid to new porous materials with high adsorption capacity. Among various adsorbents, metal–organic frameworks (MOFs) are a group of materials that have been rapidly developed and have opened new possibilities of applications, because of their excellent properties such as high surface area, high porosity, regular structure, modifiable surfaces, and tunable pore size.[12,13] Recent literature deals with the construction of MOF-based composites, and it concerns the new trend in the MOF field that consists in the construction of MOF-based composites and macro architectures in order to enhance the separation or adsorption properties of MOF.[14] Hamon et al.[15] studied the adsorption behavior of H_2S on different MOFs, including MIL-53 (Al, Cr, Fe), MIL-47(V), MIL-100(Cr), and MIL-101(Cr), and found that all compounds were able to adsorb H_2S, but reversible adsorption with a total recovery of the initial porosity was observed for MIL-53(Al, Cr) and MIL-47(V). In the case of MIL-53(Fe), destruction occurred, because of the reactive adsorption of H_2S to form iron sulfide. For MIL-100 and MIL-101, the porosity was only partially recovered, and partial destruction of the MOF was hypothesized. Further research by

Received: July 12, 2012
Accepted: September 5, 2012
Published: September 5, 2012

   dx.doi.org/10.1021/am3013104 | ACS Appl. Mater. Interfaces 2012, 4, 4942–4947

combining infrared measurements and molecular simulations showed that the MIL-47(V) structure remains rigid at H_2S pressures up to 1.8 MPa, while MIL-53(Cr) solid first presents a switch from large pores (LP) to narrow pores (NP) at very low pressure, then undergoes a second structural transition from the NP to the LP at higher pressure.[16] However, no further tests were performed to confirm and explain the assumed process of reactive adsorption, and the mechanisms of adsorption on MOFs are rarely addressed and investigated in detail when it comes to reactive adsorption.[17]

Recently, Petit and co-workers reported the synthesis of graphene oxide (GO) and MOF composites in order to increase the dispersive forces in MOF via the presence of graphene layers.[18] In this concept, GO with nonporous structure and dense arrays of layers was introduced into MOF to form composites, in order to overcome the drawback of MOFs that its void space is not beneficial for the retention of small molecules under ambient conditions, because of weak dispersive forces,[18] and the ammonia and nitrogen dioxide adsorption were also tested.[19−22] A copper-based MOF/GO was synthesized and tested for H_2S removal under ambient conditions. Compared to the parent materials, an enhancement in H_2S adsorption was found, which was due to the enhancement of physisorption in the pore space with strong dispersive forces, and reactive adsorption was also found as the main mechanism of retention.[17] Zinc oxide has been proved as an excellent adsorbent for H_2S, because of its favorable sulfidation thermodynamics and high sulfur capacity.[23] However, the GO component in the composites can induce a distortion in the structure of the MOF-5 component. Moreover, more distortion in the structure of the MOF-5 component with high amounts of GO would lead to the decrease of adsorption capacity.[20] As far as we know, there are still few works on the removal of H_2S by using Zn-based MOFs or MOF/GO composites, and there is not a clear understanding on the influence of the distortion on H_2S adsorption capacity.

In the current work, MOF-5/GO composites were synthesized with modification by glucose, and H_2S adsorption performances of the samples were measured. The influences on porosity of the composites and H_2S removal performance are discussed, and the mechanism of desulfurization is also proposed.

2. EXPERIMENTAL SECTION

2.1. Synthesis of MOF/GO Composites. GO synthesis: GO was prepared from natural graphite powder according to a modified Hummers method.[24] (See details in the Supporting Information.)

MOF-5 synthesis: zinc nitrate hexahydrate (5.2 g) and 1,4-benzenedicarboxylate (BDC, 1.0 g) were mixed in 35 mL of DMF. The mixture was treated solvothermally at 120 °C for 25 h. The obtained sample was washed with DMF and $CHCl_3$, and MOF-5 obtained by vacuum drying at 80 °C.

MOF-5/GO synthesis: GO was dispersed in *N*,*N*-dimethylformamide (DMF) solution by sonication to get DMF emulsion of GO. The glucose-promoted MOF-5/GO composites were prepared according to a modified preparation method of MOF-5.[13] In a typical reaction, zinc nitrate hexahydrate (5.2 g), BDC (1.0 g), and glucose (0.5 g) were mixed in 35 mL of GO/DMF solution. The mixture was treated solvothermally at 120 °C for 25 h. The obtained sample was washed with DMF and $CHCl_3$, and MOF-5/GOs were obtained by vacuum drying at 80 °C. Samples with GO weight ratio of 1.75%, 3.5%, 5.25%, and 7% were synthesized by changing the concentration of GO/DMF solution, and the samples are referred as MG-G*n* (*n* = 1−4), respectively. For comparison, composite with 5.25 wt % GO was also synthesized without glucose; this sample was named MG-G0.

All chemicals used are analytical purity.

2.2. Characterization of Materials. The nitrogen adsorption−desorption isotherms were performed at −196 °C using a gas adsorption analyzer (BELsorp-max, Japan). The specific surface area was evaluated using α_s plot method. The density functional theory (DFT) was used to determine the pore size distributions (PSDs). The morphologies of samples were examined by a LEO Model 1530 field-emission scanning electron microscopy (SEM) device (LEO, Oberkochen, Germany). Mid-IR spectra (4000−500 cm^{-1}) were collected on a Nicolet 560 FTIR spectrometer using pellets with samples dispersed in KBr. X-ray diffraction (XRD) analyses were carried out by using an X-ray diffractometer (Rigaku D/max-2500) with Cu Kα (40 kV, 200 mA) radiation. The data were recorded over a 2θ range of 5°−90°. X-ray photoelectron spectroscopy (XPS) was carried out by using an X-ray photoelectron spectrometer (ESCALAB250Xi, ThermoFisher) with Al Kα radiation to obtain the information of surface atomic concentration, and the binding energies were calibrated by the carbon (C 1s = 284.8 eV). The spectra obtained were curve-fitted with the nonlinear least-squares iterative technique based on the Gaussian function after baseline subtraction using Shirley's method.

2.3. Desulfurization Test. The performance of samples for H_2S removal was evaluated by the fixed-bed breakthrough test method under ambient conditions (20 °C, 1 atm). The schematic diagram is presented in Figure S1 in the Supporting Information. Before measurement, the adsorbents were crushed into particles, and the particles passed through 100-mesh sieve and were collected for the breakthrough measurement. The adsorbent particles were packed into a glass column (length of 250 mm, diameter of 6 mm) with the same length for each desulfurization test. The inlet concentration of H_2S (balance of N_2) was 100 ppmv and the flow rate was 300 mL/min. The inlet and outlet gas (H_2S) was analyzed using a gas chromatograph (Shimadzu, Model GC2014) that was equipped with a flame photometry detector (FPD). All outlet gases from the reactor were sampled with an online autosampling system and analyzed every 3 min. The breakthrough was reached when the outlet concentration was 1 ppmv. Correspondingly, the H_2S breakthrough capacity was calculated. The sample after desulfurization is named as MG-Gn-E.

3. RESULTS AND DISCUSSIONS

3.1. Morphology and Porous Structure. Figure 1 shows SEM images of the samples. MOF-5 occurred in the form of cubic crystal aggregation. The particles of GO look very dense,

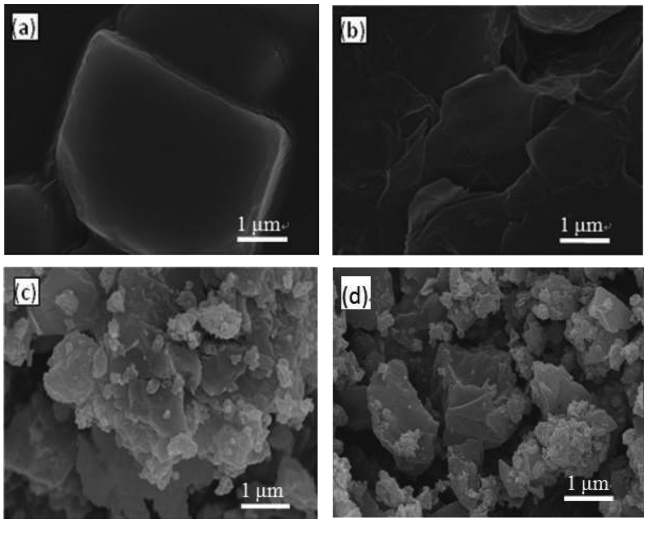

Figure 1. SEM images of (a) MOF-5, (b) GO, (c) MG-G3, and (d) MG-G4.

dx.doi.org/10.1021/am3013104 | ACS Appl. Mater. Interfaces 2012, 4, 4942−4947

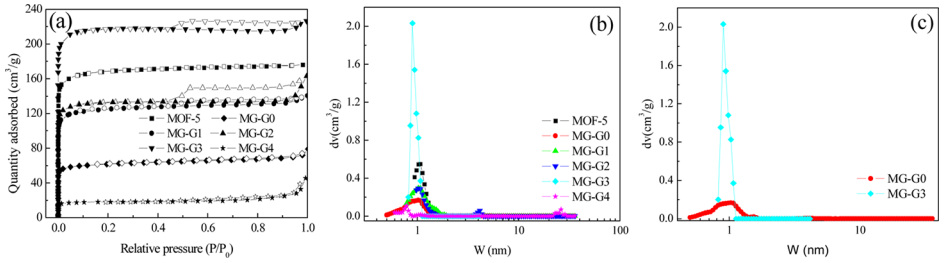

Figure 2. (a) Nitrogen adsorption−desorption isotherms and (b, c) DFT pore size distributions of samples at 77 K.

Table 1. Textural Properties and Desulfurization Performances of the Samples

sample	GO ratio (wt %)	S_{as} (m^2 g^{-1})	V_t (cm^3 g^{-1})	W_a (nm)	H_2S breakthrough time (min)	H_2S breakthrough capacity (mg/g)
GO					3	2.3
MOF-5		812	0.27	1.25	22	16.7
MG-G0	5.25	295	0.12	2.48	42	31.9
MG-G1	1.75	598	0.22	1.83	57	43.4
MG-G2	3.5	648	0.25	3.4	79	60.1
MG-G3	5.25	1062	0.35	1.64	171	130.1
MG-G4	7	86	0.07	10.5	33	25.1

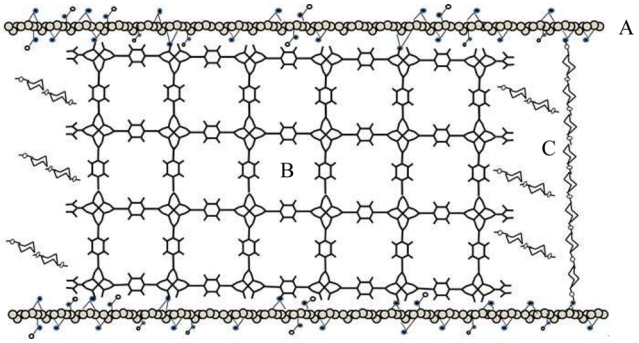

Figure 3. Schematic view of the glucose-promoted MOF-5/GO structure unit ((A) GO layer, (B) MOF-5, and (C) glucose polymer).

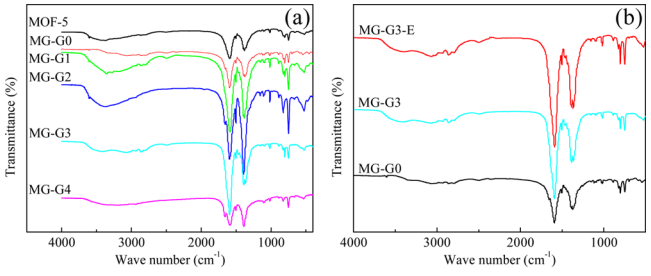

Figure 4. FTIR spectra for (a) GO, MOF-5, and MGs and (b) after desulfurization for MG-G3.

with agglomerates of graphene sheets stacked together, which can be attributed to the dispersive forces and strong specific interactions between the surface groups on the graphene-like layers.[18,19] In contrast, the MOF-5/GO consisted of thin platelets with square or round shapes, which derived from the morphology of MOF-5. With increasing GO ratio, the edges of the platelets tended to be less sharp, which is likely ascribed to more GO interference with the MOF-5 crystallization pattern.

Figure.2 shows the N_2 adsorption−desorption isotherms and PSDs for various samples with the structural parameters listed in Table 1. The isotherm of MOF-5 belongs to Type I in the IUPAC classification, which is a characteristic of microporous materials.[25] The steep rise and high N_2 uptake in the initial part

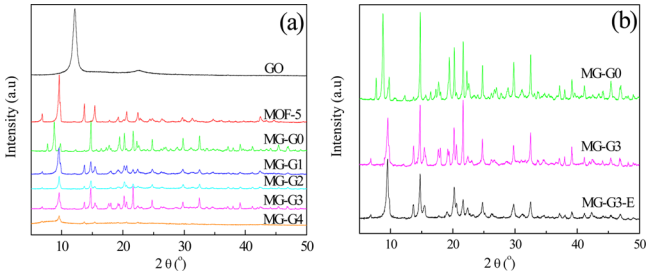

Figure 5. X-ray diffraction (XRD) patterns for the parent and composites materials (a) before and (b) after the adsorption of hydrogen sulfide (H_2S).

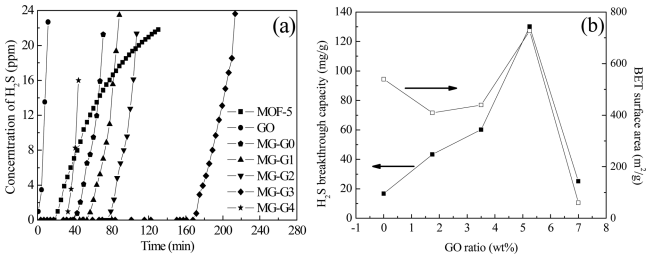

Figure 6. (a) H_2S breakthrough curves and (b) the relationship of GO ratio versus H_2S breakthrough capacity and surface area at 25 °C.

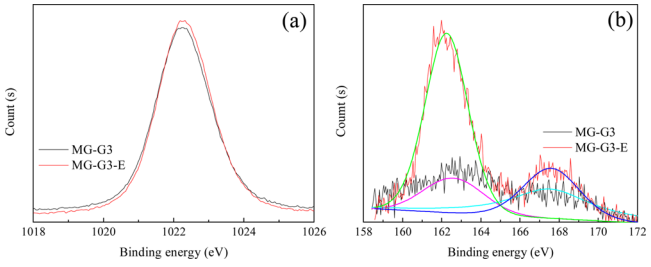

Figure 7. XPS spectra of the (a) Zn $2p_{3/2}$ and (b) S 2p narrow spectra for MG-G3 before and after desulfurization.

of the isotherm suggests the presence of a large proportion of micropores. There is not obvious hysteresis and a "tail" at the

dx.doi.org/10.1021/am3013104 | ACS Appl. Mater. Interfaces 2012, 4, 4942−4947

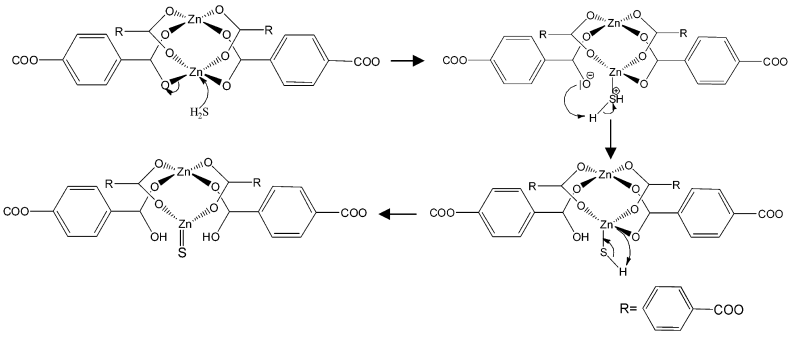

Figure 8. Mechanism of the desulfurization process of MOF-5/GO composites.

high-relative-pressure region, indicating that the amount of mesopores or macropores is very few. Type H4 hysteresis loops are observed for MGs, indicating the presence of a small amount of mesopores. The hysteresis loop is broadened with increasing GO ratio up to 3.5% and then becomes smaller with further increasing GO ratio. However, an excessive addition of GO would lead to the destruction of the pore structure. All MOF-5/GO samples show a "tail" appearing at P/P_0 close to 1, suggesting that there are some large mesopores or macropores, which are likely to be the pores between the units of MOF-5/GO, and their sizes could be limited by the sizes of GO flakes. It is worthwhile to note that the N_2 uptake of MG-G4 is much lower than other MGs, revealing the poor porosity and low surfaces area of this sample.

Figure 2b shows the PSDs of the samples. All samples possess roughly similar, multimodal PSDs with distinct maxima in the micropore region. Very weak peaks are observed in the range of 4−5 nm. For MG-G4, some large mesopores appear at 20−30 nm, which correspond to the "tail" at high relative pressure. From Table 1, it can be seen that the surface areas of MG-G1 and MG-G2 are lower than MOF-5, which may be related to the destruction of partial pore structure by GO with layer structure. This can be proved by the hysteresis loop H4, which is a characteristic of slit pores.[25] In addition, blockage by polymers derived from partially solvothermal carbonation of glucose may be another reason. It is interesting to note that MG-G3 with 5.25 wt % GO exhibits more developed porous structure than MOF-5. Unfortunately, with a higher content of GO, the beneficial effect on porosity vanished, leading to a sharp decrease in surface area for MG-G4. Therefore, it is postulated that the developed pore structure for MG-G3 could be attributed to the well synergy effects between GO and MOF-5.

In order to clarify the effect of glucose on porous structure, a sample (MG-G0) with 5.25 wt % GO was also synthesized without using glucose. It can be seen from Table 1 that MG-G0 has a much lower surface area than other samples, except MG-G4. That is to say, without the introduction of glucose, there would be an undesirable influence of GO on porous structure. It is reported that a polymerization process for glucose would occur when treated by hydrothermal reaction below 140 °C,[26] and polymers formed have a low degree of polymerization.[24] Some polymers may fill in the structure to support the framework, and some may react with the functional groups on the GO (Figure 3). In addition, Figure 2c shows that, with the addition of glucose, the PSD of the MOF-5/GO composite is narrowed, with a sharp peak centered at ca. 1 nm. Therefore, glucose enhances the porous structure of the composites to some extent, because of its hindrance on GO's distortion effect. With 5.25 wt % GO, the composite can get a good match between GO and glucose to achieve the highest surface area. However, an overloading of GO up to 7 wt % may destroy this type of matching, leading to a very low surface area.

3.2. FTIR Analysis. Figure 4 shows the FTIR spectra for the samples. Several bands are observed in the region of 700−1300 cm^{-1}, which are assigned to the fingerprint region and the out-of-plane vibrations of BDC.[20,27] The bands in the region of 750−875 cm^{-1} are assigned to aromatic C−H out-of-plane bending vibrations,[28] while the bands in the 1000−1450 cm^{-1} correspond to C−O (hydroxyl, ester, or ether) stretching and O−H bending vibrations.[29] The band at 1390 cm^{-1} is due to the symmetric stretching of carboxylic groups in BDC, whereas those at 1510 and 1590 cm^{-1} are attributed to the asymmetric stretching of carboxylic groups in BDC.[20] A broad band at 3000−3700 cm^{-1} must be due to the overlapping bands from O−H (hydroxyl or carboxyl), whereas the bands at 2855 and 2922 cm^{-1} correspond to stretching vibrations of aliphatic C−H.[19,30] These results indicate that there are a large number of residues including hydroxyl and carboxyl groups on the surface of the as-prepared materials. It can be also seen that the intensity of adsorption bands becomes stronger with the GO ratio up to 3.5% and then tends to be weaker with further increasing of GO ratio, indicating that the amount of functional groups follows the same trend. These functional groups can provide a potential avenue to load other functional groups, molecules, ions, and nanoparticles.[29] In addition, there is not obvious difference between the IR spectra of MOF-5 and MG-G0, indicating that GO almost does not have any influence on the surface chemistry of the composites. However, when glucose is introduced, the intensity of bands in the range of 1000−1300 cm^{-1}, which include the C−OH stretching and OH bending vibrations,[24] tends to be stronger, suggesting the existence of large numbers of residual hydroxy groups in the composites.

After H_2S adsorption, significant changes in the vibration bands can be observed. The intensity of all bands is much stronger after desulfurization, which can be attributed to the H_2S adsorption process, during which the adsorption of H_2S leads to a release of the BDC ligands. In addition, the significant enhancement of bands at 660−1600 cm^{-1} must be due to the collapsing of the MOF-5 structure and change in the environment of carboxylic groups and zinc oxide.[19] Furthermore, the bands at 2510 cm^{-1} observed on the spectra of the exhausted samples can also be attributed to S−H stretching vibrations in H_2S species, and this band generally exhibits a very weak IR intensity and can sometimes be missed.[31]

3.3. XRD Analysis. Figure 5 shows the X-ray diffraction (XRD) patterns of the samples before and after H_2S

dx.doi.org/10.1021/am3013104 | ACS Appl. Mater. Interfaces 2012, 4, 4942−4947

adsorption. The GO spectrum shows a peak at 2θ = 12.1°, indicating an interlayer distance of 7.3 Å. It suggests that the as-prepared GO has a high degree of orientation.[32,33] The diffraction pattern of MOF-5 is in agreement with those found for well-defined MOF-5 crystals,[34] suggesting that the current material has the expected structure. The MOF/GO sample (MG-G0) synthesized without using glucose exhibits a significant splitting at 9.7°, indicating that the GO component in the composites induces a distortion in the structure of the MOF-5 component.[20,34] Interestingly, this splitting disappears when glucose is used in the synthesis process, the diffraction patterns of the MOF-5/GO composites are similar to that observed for MOF-5, which indicates that the MOF-5 structure is preserved. These results suggest that glucose can sustain the crystal structure of MGs similar as MOF-5, avoiding the distortion caused by GO. It is noticeable that the relative intensity of the XRD pattern for MG-G4 tends to be much weaker, revealing that a higher content of GO still distorts the crystal structure. After exposure to H_2S, the spectra are slightly modified and the strength of the diffraction peaks becomes weaker, but the overall patterns are preserved. These results suggest that exposure to H_2S causes the partial collapse of the MOF-5 structure, because of the reactions of H_2S with the MOF-5 units.

3.4. Desulfurization Performance. The desulfurization would be a process consisting of both physical adsorption and chemical reaction. The H_2S breakthrough curves, the relationship of GO ratio vs H_2S breakthrough capacity, and the specific surface area for various adsorbents are illustrated in Figure 6. The breakthrough capacities are summarized in Table 1. The breakthrough times for GO and MOF-5 are very short (ca. 3 and 22 min, respectively), indicating that GO and MOF-5 are poor adsorbents for H_2S, although MOF-5 possesses a high specific surface area. In contrast, the breakthrough time of MG-G0 is much longer than that of GO and MOF-5. This can be attributed to an increase in the dispersive forces required to retain H_2S, because of the additional GO component.[18,19] Moreover, the breakthrough times of MOF-5/GO composites modified by glucose are even longer than that of MG-G0. From Table 1, the order in terms of adsorption capacity is listed:

$$\text{MG-G3} \gg \text{MG-G2} > \text{MG-G1} > \text{MG-G0} > \text{MG-G4} > \text{MOF-5} > \text{GO}$$

which suggests that the modification by glucose leads to a significant enhancement for H_2S removal. These results suggest that the distortion in MOF-5 by GO is beneficial for H_2S adsorption. However, with higher amounts of GO, more distortion in the structure of the MOF-5 leads to a decrease in the amount of H_2S adsorbed.[20] Under this circumstance, the introduction of glucose can promote the H_2S adsorption of the MOF-5/GO composites due to the structural support and hindrance on more structural distortion. It should be pointed out that a good match between GO and glucose can have the well synergy effect. For MG-G3, it has more developed pore structure and increased dispersive forces to retain H_2S.

As Figure 5b shows, the H_2S breakthrough capacities of MOF-5/GO composites first increased sharply with increasing GO ratio up to 5.25 wt %, and then decreased dramatically with further loading. The sample MG-G3 exhibits a super affinity to H_2S and the breakthrough capacity reached 130.1 mg/g. It also can be seen that the H_2S breakthrough capacity follows the same tread as the specific surface area, except for MOF-5 (which is free of GO), indicating that the H_2S adsorption capacity is highly dependent on the porosity of the samples. However, the high surface area and low H_2S adsorption capacity for MOF-5 demonstrates that the porosity of the materials is not the only factor governing the desulfurization capacity. That is to say, the desulfurization process is influenced not only by physisorption, but also by chemical reaction. Moreover, it is worthy to point out that the breakthrough time not only depends on the micro/mesoscopic and surface characteristics of the materials, but also tightly relates to the macroscopic aspect of the materials (size and shape of the grains) packed into the glass column, which affect the diffusion kinetics of the analytes through the column. Therefore, it is difficult to assign the different desulfurization performances to the specific aspects exactly.

Figure 7 shows the XPS narrow spectra of Zn $2p_{3/2}$ and S 2p for MG-G3 before and after desulfurization. High-resolution XPS curves in the region of 1020−1025 eV in Figure 7a show an intense peak at a binding energy (BE) of 1022.5 eV, which is a characteristic of the $2p_{3/2}$ transition of ZnO.[35] A slight change is observed after desulfurization, which indicates that the exposure to H_2S does not have any influence on the chemical environment of zinc, because there is a similar status between ZnO and ZnS. In Figure 7b, two BE peaks over 162.1 and 168 eV of S 2p are observed, which are usually related to sulfur in sulfide and sulfate, respectively.[36] The existence of sulfate would be a consequence of sulfuric acid treatment in the GO preparation process, and the sulfide can be attributed to the formation of sulfur-containing species in the chemical reaction between H_2S and the MOF-5/GO composites. It can be seen that the intensity of the S 2p curves becomes much stronger after desulfurization, and, as expected, the atomic concentration of sulfur increases from 0.06% in the fresh sample to 1.36% in the sample after desulfurization (see Table S1 in the Supporting Information). XPS only gives the surface atomic percentage of materials, while the adsorption of H_2S occurs not only on the surface, but also in the bulk of the materials. Besides, the physical adsorption of H_2S could not be detected via XPS. Therefore, the low atomic concentration of S in the sample was obtained by XPS after the removal of H_2S.

Based on the characterization of nitrogen adsorption, IR, XRD and XPS, and considering the reaction mechanism of H_2S with copper-based metal−organic framework and graphene oxide composites,[17] the chemical reaction of H_2S with the MOF-5/GO composites was supposed, as shown in Figure 8. H_2S binds to the Zn sites by successive reactions, which leads not only to the formation of carboxylic acid and ZnS, but also to a change in the coordination between Zn and O in BDC. These results can be confirmed by the fact that the bands are significantly enhanced in the FTIR spectra, especially for the band at ∼1590 cm^{-1}, which is ascribed to the "release" of carboxylic groups during the collapsing of MOF-5 structure.[19] During the process, the bond breaking results in the collapse of the MOF-5 structure and a decrease in the porosity.

Generally speaking, as the number of available Zn site increases, the possibility for H_2S to be adsorbed to form sulfur-containing species increases, resulting a corresponding increase in the adsorption capacity. It is likely that a small amount of GO not only creates pore space with strong dispersive forces where H_2S can be strongly retained, but also increases available Zn sites of MOF-5. However, more GO loading would cause more distortion and even destroy the pore structure, leading to the decrease of H_2S adsorption capacity. The introduction of

glucose can support the structural stability and hinder more structural distortion, thus promote the H_2S adsorption by enhancing both the physisorption and the reactive adsorption.

4. CONCLUSIONS

Glucose-modified MOF-5/GO composites are synthesized using the solvothermal method. The loading of graphene oxide makes a contribution to the enhancement of dispersive force in MOF-5 but leads to distortion in the crystal structure. The introduction of glucose can restrain more distortion to support the structural stability. For the modified composites, the surface area first increases and then decreases with increasing GO ratio, and the H_2S adsorption capacity follows the same changing trend with the maximum uptakes of 130.1 mg/g. A good match between GO and glucose leads to a developed porous structure, resulting in the highest H_2S adsorption capacity by enhancing both the physisorption and the reactive adsorption.

■ ASSOCIATED CONTENT

Ⓢ Supporting Information

Experimental and characterization details. This information is available free of charge via the Internet at http://pubs.acs.org/.

■ AUTHOR INFORMATION

Corresponding Author

*Tel.: 0086 10 62773752. Fax: 0086 10 62771160. E-mail: zhhuang@tsinghua.edu.cn (Z.-H.H.), fykang@tsinghua.edu.cn (F.K.).

Present Address

[§]Blue Star (Beijing) Chemical Machinery Co., Ltd., Beijing 100176, People's Republic of China.

Notes

The authors declare no competing financial interest.

■ ACKNOWLEDGMENTS

The authors are grateful for the financial support from the National High Technology Research and Development Program of China (863 Program, No. 2010AA064907).

■ REFERENCES

(1) Syed, M.; Soreanu, G.; Falletta, P.; Beland, M. *Can. Biosyst. Eng.* **2006**, *48*, 1−14.

(2) Henshaw, P.; aaMedlar, D.; McEwen, J. *Water Res.* **1999**, *33*, 3107−3110.

(3) Liu, B. S.; Wei, X. N.; Zhan, Y. P.; Chang, R. Z.; Subhan, F.; Au, C. T. *Appl. Catal., B* **2011**, *102*, 27−36.

(4) Chung, Y. C.; Huang, C. P.; Tseng, C. P. *Chemosphere* **2001**, *43*, 1043−1050.

(5) Belmabkhout, Y.; Heymans, N.; De Weireld, G.; Sayari, A. *Energy Fuels* **2011**, *25*, 1310−1315.

(6) Primavera, A.; Trovarelli, A.; Andreussi, P.; Dolcetti, G. *Appl. Catal., A* **1998**, *173*, 185−192.

(7) Bandosz, T. J.; Block, K. A. *Ind. Eng. Chem. Res.* **2006**, *45*, 3666−3672.

(8) He, R.; Xia, F.-F.; Wang, J.; Pan, C.-L.; Fang, C.-R. *J. Hazard. Mater.* **2011**, *186*, 773−778.

(9) Wang, W.; Peng, X.; Cao, D. *Environ. Sci. Technol.* **2011**, *45*, 4832−4838.

(10) Mu, B.; Walton, K. S. *Adsorption* **2011**, *17*, 777−782.

(11) Zhao, Z.; Li, X.; Li, Z. *Chem. Eng. J.* **2011**, *173*, 150−157.

(12) Furukawa, H.; Ko, N.; Go, Y. B.; Aratani, N.; Choi, S. B.; Choi, E.; Yazaydin, A. O.; Snurr, R. Q.; O'Keeffe, M.; Kim, J.; Yaghi, O. M. *Science* **2010**, *329*, 424−428.

(13) Hafizovic, J.; Bjørgen, M.; Olsbye, U.; Dietzel, P. D. C.; Bordiga, S.; Prestipino, C.; Lamberti, C.; Lillerud, K. P. *J. Am. Chem. Soc.* **2007**, *129* (12), 3612−3620.

(14) Reboul, J.; Furukawa, S.; Horike, N.; Tsotsalas, M.; Hirai, K.; Uehara, H.; Kondo, M.; Louvain, N.; Sakata, O.; Kitagawa, S. *Nat. Mater.* **2012**, *11*, 717−723.

(15) Hamon, L.; Serre, C.; Devic, T.; Loiseau, T.; Millange, F.; Ferey, G.; De Weireld, G. *J. Am. Chem. Soc.* **2009**, *131*, 8775−8777.

(16) Hamon, L.; Leclerc, H.; Ghoufi, A.; Oliviero, L.; Travert, A.; Lavalley, J.-C.; Devic, T.; Serre, C.; Ferey, G.; De Weireld, G.; Vimont, A.; Maurin, G. *J. Phys. Chem., C* **2011**, *115*, 2047−2056.

(17) Petit, C.; Mendoza, B.; Bandosz, T. J. *ChemPhysChem* **2010**, *11*, 3678−3684.

(18) Petit, C.; Bandosz, T. J. *Adv. Mater.* **2009**, *21*, 4753−4757.

(19) Petit, C.; Bandosz, T. J. *J. Mater. Chem.* **2009**, *19*, 6521−6528.

(20) Petit, C.; Bandosz, T. J. *Adv. Funct. Mater.* **2010**, *20*, 111−118.

(21) Petit, C.; Huang, L.; Jagiello, J.; Kenvin, J.; Gubbins, K. E.; Bandosz, T. J. *Langmuir* **2011**, *27*, 13043−13051.

(22) Levasseur, B.; Petit, C.; Bandosz, T. J. *ACS Appl. Mater. Interfaces* **2010**, *2*, 3606−3613.

(23) Dhage, P.; Samokhvalov, A.; Repala, D.; Duin, E. C.; Tatarchuk, B. J. *Phys. Chem. Chem. Phys.* **2011**, *13*, 2179−2187.

(24) Tang, Z.; Shen, S.; Zhuang, J.; Wang, X. *Angew. Chem., Int. Ed.* **2010**, *49*, 4603−4607.

(25) Rouquerol, J.; Rouquerol, F.; Sing, K. S. W. In *Adsorption by Powders and Porous Solids: Principles, Methodology and Applications*. Academic Press: San Diego, 1999; Vol. *1*, p 99.

(26) Sun, X. M.; Li, Y. D. *Angew. Chem., Int. Ed.* **2004**, *43*, 597−601.

(27) Hermes, S.; Schroder, F.; Amirjalayer, S.; Schmid, R.; Fischer, R. A. *J. Mater. Chem.* **2006**, *16*, 2464−2472.

(28) Lua, A. C.; Yang, T. *J. Colloid Interface Sci.* **2004**, *274*, 594−601.

(29) Zheng, M.; Liu, Y.; Jiang, K.; Xiao, Y.; Yuan, D. *Carbon* **2010**, *48*, 1224−1233.

(30) Sevilla, M.; Fuertes, A. B. *Chem.—Eur. J.* **2009**, *15*, 4195−4203.

(31) Lin-Vien, D.; Colthup, N. B.; Fateley, W. G.; Grasselli, J. G. In *The Handbook of Infrared and Raman Characteristic Frequencies of Organic Molecules*; Academic Press: New York, 1991; Vol. *1*, p 112.

(32) Seredych, M.; Tamashausky, A. V.; Bandosz, T. J. *Adv. Funct. Mater.* **2010**, *20*, 1670−1679.

(33) Xu, Y.; Sheng, K.; Li, C.; Shi, G. *ACS Nano* **2010**, *4*, 4324−4330.

(34) Hafizovic, J.; Bjorgen, M.; Olsbye, U.; Dietzel, P. D. C.; Bordiga, S.; Prestipino, C.; Lamberti, C.; Lillerud, K. P. *J. Am. Chem. Soc.* **2007**, *129*, 3612−3620.

(35) Chaturvedi, S.; Rodriguez, J. A.; Hrbek, J. *J. Phys. Chem. B* **1997**, *101*, 10860−10869.

(36) Moulder, J. F.; Stickle, W. F.; Sobol, P. E.; Bomben, K. D. In *Handbook of X-ray Photoelectron Spectroscopy*. Perkin−Elmer Corp.: Eden Prairie, MN, 1992; Vol. *1*, p 61.